

# Clustering of activated microglia occurs before the formation of dystrophic neurites in the evolution of A $\beta$ plaques in Alzheimer's disease.

Patrick Jarmo Paasila<sup>2</sup>, Danielle Suzanne Davies<sup>1</sup>, Greg Trevor Sutherland<sup>2</sup>, Claire Goldsbury<sup>1</sup>

<sup>1</sup> *Discipline of Anatomy and Histology, School of Medical Sciences, Faculty of Medicine and Health, The University of Sydney, NSW 2006, Australia*

<sup>2</sup> *Discipline of Pathology, School of Medical Sciences, Faculty of Medicine and Health, The University of Sydney, NSW 2006, Australia*

Corresponding author:

Dr Claire Goldsbury PhD · Brain and Mind Centre · 94 Mallett Street · Camperdown, NSW 2050 · Australia · Tel +61 2 9351 0878  
[claire.goldsbury@sydney.edu.au](mailto:claire.goldsbury@sydney.edu.au)

Submitted: 16 June 2020 · Accepted: 29 July 2020 · Copyedited by: Jeffrey Nirschl · Published: 04 August 2020

## Abstract

Alzheimer's disease (AD) is a late-onset disease that has proved difficult to model. Microglia are implicated in AD, but reports vary on precisely when and how in the sequence of pathological changes they become involved. Here, post-mortem human tissue from two differentially affected regions of the AD brain and from non-demented individuals with a high load of AD-type pathology (high pathology controls) was used to model the disease time course in order to determine how microglial activation relates temporally to the deposition of hallmark amyloid- $\beta$  (A $\beta$ ) and hyperphosphorylated microtubule associated protein tau pathology. Immunofluorescence against the pan-microglial marker, ionised calcium-binding adapter molecule 1 (IBA1), A $\beta$  and tau, was performed in the primary motor cortex (PMC), a region relatively spared of AD pathological changes, and compared to the severely affected inferior temporal cortex (ITC) in the same cases. Unlike the ITC, the PMC in the AD cases was spared of any degenerative changes in cortical thickness and the density of Betz cells and total neurons. The clustering of activated microglia was greatest in the PMC of AD cases and high pathology controls compared to the ITC. This suggests microglial activation is most prominent in the early phases of AD pathophysiology. Nascent tau inclusions were found in neuritic plaques in the PMC but were more numerous in the ITC of the same case. This shows that tau positive neuritic plaques begin early in AD which is likely of pathogenic importance, however major tau deposition follows the accumulation of A $\beta$  and clustering of activated microglia. Importantly, findings presented here demonstrate that different states of microglial activation, corresponding to regional accumulations of A $\beta$  and tau, are present simultaneously in the same individual; an important factor for consideration if targeting these cells for therapeutic intervention.

**Keywords:** Alzheimer's disease, Inferior temporal cortex, Microglia, Post-mortem human brain tissue, Primary motor cortex

## Introduction

Alzheimer's disease (AD) is neuropathologically characterised by inclusions of microtubule-associated protein tau (tau) and extracellular deposits of  $\beta$ -amyloid (A $\beta$ ). Intraneuronal tau pathology includes neurofibrillary tangles (NFTs) in the cell soma and neuropil threads (NTs), which occur mostly in the dendritic compartment, but also in the axonal domain though to a lesser extent (1, 2). NFTs and NTs are both comprised of paired helical filaments and straight filaments of polymerised hyperphosphorylated tau protein (3, 4). The extent of tau pathology follows a predictable spatiotemporal progression through functionally integrated brain regions (5, 6) and there is an extensive body of literature that demonstrates an inverse correlation between the accumulation of NFTs and cognitive status (7) such that the spread and regional level of NFTs reflects the severity of dementia with time (8).

Contrastingly, A $\beta$  plaques follow a seemingly more haphazard regional pattern of accumulation throughout the neocortex, indeed plateauing relatively early in the disease time course (9, 10), and therefore correlate poorly with disease status until substantial argyrophilic neuritic tau pathology is also present (5, 7, 11). Whilst A $\beta$  load may be an unreliable indicator of disease severity, it is generally accepted that the extent of its spread, in combination with tau pathology, is useful for staging purposes (9). A $\beta$  plaques can be classified with immunostaining into at least three morphologically distinct categories: diffuse, fibrillar, or dense-cored. Diffuse plaques have long been proposed to be a structural precursor of other plaque forms, but whether these categories represent separate entities with independent mechanisms of development or are temporally linked is still unclear. Neuritic plaques (NPs) are those A $\beta$  plaques that also feature dystrophic neurites (DNs) with silver staining. DNs can occur in all these morphological subtypes of A $\beta$  plaques, though more commonly in dense-cored and fibrillar plaques than morphologically diffuse plaques (12). Most DNs are tau-positive and morphologically similar to NTs which are elongated in shape, but may also be globular, and possibly represent swollen presynaptic (axonal) terminals

(13). NPs that retain sparse DNs but show minimal A $\beta$  staining have previously been described and were termed 'remnant plaques' which were proposed to result from glial phagocytosis of insoluble A $\beta$  (14).

There remains significant debate as to the sequence of the neuropathological changes that precede the onset of AD symptomatology. The amyloid cascade hypothesis posits A $\beta$ , and in particular the soluble, oligomeric, non-fibrillar fraction, as the initiating factor (15-20). A competing view is offered by others who contend that the sequence of pathological events begins with neurofibrillary pathology (21, 22) which precedes the formation of insoluble A $\beta$  pathology (23). Indeed, there is evidence that tau pathology occurs prior to A $\beta$  pathology as it is more common in the brains of non-demented individuals (21) but this might represent a non-AD scenario described as primary age-related tauopathy (PART) (24). Notwithstanding the order of events, both hypotheses suggest that an activated glial response is an integral component of the pathogenesis of AD.

The study of microglia morphology in post-mortem human brain tissue presents a simple method with which to gauge the involvement of microglia in instances of changed physiological conditions or to the development of a disease. Microglia with a ramified morphology, characterised by thin, evenly distributed, highly branched processes with a small, spherical soma, represent the healthy cell population (25-27). Activated microglia are characterised by reduced morphological complexity including hypertrophy of the soma and processes and may also display the formation of distal phagosomes (23, 25, 28). Dystrophic microglia display features consistent with cellular senescence (29), including a loss of processes, tortuosity of remaining processes, and discontinuous IBA1-immunolabelling (30-32). Lastly, clusters of activated microglia in AD have been noted previously in post-mortem human brain tissue and represent the direct interaction between microglia and A $\beta$  and tau pathology (10, 32, 33).

By investigating brain regions differentially affected by AD-type pathology in non-demented and demented individuals it may be possible to model the sequence of pathological changes in the dis-

ease, in particular the activated microglial response. Previously we demonstrated an increased density of activated microglia in the inferior temporal cortex (ITC) of non-demented controls with similar levels of AD-type pathology ('high pathology controls' – HPCs) as clinically and neuropathologically-confirmed AD cases (26). This suggested that the microglial response occurs in the preclinical phases of AD but we wished to confirm this finding in a belatedly affected region of the AD brain, the primary motor cortex (PMC), compared to an earlier and more severely affected region, the ITC, of the same cases. Further, we wished to determine the sequence of A $\beta$ , tau, and microglia pathological changes that occur in the cortex. The findings here

demonstrate that nascent NTs and DNs in the PMC begin early in the pathogenesis of AD, but follow the clustering of activated microglia. By contrast, looking at the severely affected ITC in the same cases, findings suggest that microglial clustering at plaques dissipates once tau and A $\beta$  pathology is long established and there is also a substantial loss of IBA1-immunoreactivity (26, 34). Although an early toxic microglial gain of function cannot be ruled out, these findings appear most consistent with a scenario where microglial activation is neuroprotective early in the pathogenesis of AD. We suggest that this is followed by a gradual exhaustion of microglial function that contributes to cognitive deterioration in the AD brain.

**Table 1. Cohort characteristics.**

Case ID	Age	Sex	Status	Cause of death	AD duration (years)	CDR	ABC score	AD likelihood
M03	76	Female	AD	Cardiorespiratory failure	11	3	A3 B2 C3	Intermediate
M04	77	Male	AD	Aspiration pneumonia	9	2	A3 B3 C2	High
M09	80	Female	AD	Alzheimer's disease	10	3	A3 B3 C3	High
M11	83	Male	AD	Cerebrovascular	5	3	A3 B3 C3	High
M12	83	Female	AD	Uraemia	7	3	A3 B3 C2	High
M13	84	Female	AD	Aspiration pneumonia	13	3	A3 B3 C3	High
M17	85	Female	AD	Cardiorespiratory failure	5	3	A3 B3 C3	High
M22	98	Female	AD	Cerebrovascular	6	3	A3 B3 C2	High
M14	85	Male	HPC	Cancer	-	-	A2 B2 C3	Intermediate
M18	87	Female	HPC	Cancer	-	-	A2 B2 C0	Intermediate
M19	92	Female	HPC	Pancytopenia	-	0	A2 B2 C2	Intermediate
M21	87	Female	HPC	Acute peritonitis	-	0	A3 B2 C1	Intermediate
M23	102	Female	HPC	Acute renal failure	-	0	A2 B2 C2	Intermediate
M01	69	Male	Control	Cardiac failure	-	-	A3 B1 C3	Low
M02	74	Female	Control	Cancer	-	-	A3 B1 C3	Low
M05	78	Female	Control	Respiratory failure	-	-	A0 B0 C0	Not
M06	78	Female	Control	Toxicity	-	-	A0 B1 C0	Not
M07	81	Male	Control	Cardiac failure	-	-	A0 B2 C0	Not
M08	80	Male	Control	Respiratory failure	-	-	A0 B0 C0	Not
M10	82	Female	Control	Respiratory failure	-	-	A3 B1 C2	Low
M15	85	Female	Control	Respiratory failure	-	-	A2 B1 C0	Low
M16	85	Female	Control	Pneumonia	-	0	A2 B0 C1	Low
M20	93	Female	Control	Cardiac failure	-	0.5	A1 B0 C0	Low

## Methods

This study was approved by the University of Sydney's Human Research Ethics Committee (HREC#2015/477). All tissue samples for this study, as well as demographic and clinical information, were supplied by the New South Wales Brain Tissue Resource Centre (NSWBTRC) and the Sydney Brain Bank (SBB), collectively the New South Wales Brain Banks (NSWBB), following approval from their Scientific Advisory Committee. Methods for case ascertainment and tissue preparation by NSWBB have been previously published (35). The demographic and clinicopathological characteristics of the cohort (Table 1) and data from the ITC have been previously published (26).

### Immunofluorescence

Immunofluorescence staining procedures were performed on free-floating 45  $\mu\text{m}$  fixed sections derived from the caudal aspect of the superomedial area of the PMC of controls ( $n = 10$ ), HPCs ( $n = 5$ ), and pathologically confirmed AD cases ( $n = 8$ ) as previously described (26). Double-labelled sections using antibodies against A $\beta$ , total tau (TTau), and the pan-microglial marker ionised calcium-binding adapter molecule 1 (IBA1), were used for the quantification of A $\beta$  and tau loads and microglial morphological subtypes.

For A $\beta$  and IBA1 quantification, heat-induced epitope retrieval was performed using a sodium citrate solution (pH 8.5) at 60°C overnight, followed by a 12-minute formic acid (90%) incubation at room temperature. Blocking was performed in 10% normal goat serum (Gibco #16210072), and primary (mouse A $\beta$ , 1:1000, BioLegend 803002; rabbit IBA1, 1:1000, Wako 019-19741) and secondary (1:200; Thermo Scientific: Alexa Fluor (AF) 488 goat anti-mouse, #A11001; AF 568 goat anti-rabbit, #A11011) antibody incubations were performed at 4°C with gentle agitation. Nuclear counterstaining was performed in the last 40 minutes of the secondary antibody incubation by the addition of Hoechst 33342 dye (1  $\mu\text{g}/\text{mL}$ ; Thermo Scientific 62249). Sections were mounted using Prolong Diamond Antifade (Invitrogen P36961). Double-immunolabelling of TTau (rabbit; 1:500; Dako K9JA/A0024) and IBA1 (mouse; 1:50; Millipore

MABN92) was carried out as previously described (34). TTau immunostaining of NFTs, NTs, and DNAs has previously been demonstrated to give comparable immunostaining to standard phosphotau antibodies (12E8 and AT8) (36). Briefly, heat-retrieval was performed with sodium citrate (pH 6.0) for 10 minutes at 100°C, before permeabilising, blocking with BSA, and incubating in primary antibodies for three hours at room temperature or overnight at 4°C, and finally incubating in secondary antibodies (1:200; Invitrogen: AF555 goat anti-mouse, A214424; AF647 goat anti-rabbit, A21244). Hoechst 33342 was added to counterstain nuclei and sections were mounted in ProLong Gold Antifade.

### Image acquisition and analysis

A $\beta$  and IBA1 double-labelled sections were imaged using a Zeiss LSM 800 confocal microscope using the 'tile scan' function at the Advanced Microscopy Facility, Bosch Institute, The University of Sydney. A previously validated modified disector sampling approach that utilises one section per individual was used here for the analysis of the A $\beta$  and IBA1 immunostained sections (37). Briefly, a total of three cortical strips per section from areas where the pial surface and the grey-white boundary were strictly in parallel were acquired for the quantification of microglia, A $\beta$  plaques and A $\beta$ -positive pixels. These cortical strips were constructed of serial images 500  $\mu\text{m}$  in width, 6  $\mu\text{m}$  in z-depth with three z-slices (z-step = 3  $\mu\text{m}$ ), spanning all of the cortical laminae of the PMC using a 20 $\times$ /0.8 numerical aperture (NA) objective. Clusters of microglia and individual microglia, which were categorised as having either a ramified, activated, or dystrophic morphology as previously described (26), were enumerated in image analysis software (Fiji; NIH). The terminology used to describe the different populations of morphologically diverse populations of microglia was informed by previous investigations (25, 28, 30). Microglia with thin, highly branched processes, and a spherical nucleus were categorised as 'Ramified'. 'Activated' microglia (previously termed 'deramified' (34)) included those cells that displayed hypertrophy of the soma or processes with retraction of secondary or tertiary processes. 'Dystrophic microglia' were identified on the basis of a loss of processes with the

remaining processes displaying significant tortuosities or discontinuous IBA1-immunolabelling with or without blebbing or punctate IBA1-labelling (previously dystrophic microglia were subcategorised as either 'punctate' or 'discontinuous' to reflect these observations (34)). A 'Cluster of microglia' was counted if three or more soma occurred within, or were touching the margins of, a 20  $\mu\text{m}^2$  virtual graticule subregion. Larger clusters were counted as one cluster if the graticule subregion could be moved and still incorporate at least three somata. Clusters were counted whilst visualising only the 568 nm (IBA1-positive) channel to distinguish these from individual microglia and to minimise potential false-positive counts in the presence of either A $\beta$ - or T Tau-immunostaining. The total number of microglia counted per section averaged 519 with a coefficient of error (CE) of  $\leq 0.2$  for all counts of morphological subtypes, with the exception of microglial clusters (CE  $\leq 0.3$ ) which were relatively rare and displayed significant variance between cases.

Quantification of T Tau was carried out using an Olympus VS120 slide scanner at the Sydney Microscopy and Microanalysis, Brain and Mind Centre, The University of Sydney. Whole section DIC and fluorescence overviews of a single section from each case were generated using a 10 $\times$  objective and were used to systematically map out four representative 500  $\mu\text{m}^2$  regions of interest (= 1mm<sup>2</sup> per section) within the mid-cortical laminae (III-V) for manual counts of NFTs and for the quantification of T Tau-positive pixels. Individual images were captured using a 40 $\times$ /0.9 NA objective and were comprised of seven z-slices with a depth of 6  $\mu\text{m}$  (z-step = 1  $\mu\text{m}$ ). Image analysis was performed in Fiji using manually thresholded images. Positive pixel counts were generated for A $\beta$  and T Tau staining and expressed as a percentage of total pixels (% A $\beta$  and % T Tau respectively). High resolution imaging of all immunolabelled sections were carried out using a Nikon A1R or Zeiss LSM 710 confocal microscope (Sydney Microscopy and Microanalysis, Charles Perkins Centre and Brain and Mind Centre, The University of Sydney). Features were imaged with either a 40 $\times$ /0.95 NA or 100 $\times$ /1.4 NA objective and shown as maximum intensity projections.

### Nissl staining

Nissl stains of free-floating 45  $\mu\text{m}$  thick formalin-fixed sections were performed for the meas-

urement of cortical thickness and neuronal counts. Sections were incubated in 0.1% cresyl violet acetate (0.02% glacial acetic acid; added immediately before use) for 15 minutes at 60°C. Differentiation was achieved by sequentially washing sections for three minutes in 70% and 95% ethanol. The final level of staining was adjusted by briefly dipping sections in 100% ethanol and confirmed by light microscopy before clearing in xylene for ten minutes and mounting in DPX. Cortical thickness measurements and neuronal counts were performed on three cortical strips from one section per individual using an eyepiece graticule on an Olympus BX50 microscope using a 20 $\times$ /0.75 NA objective. A height measure of 45  $\mu\text{m}$  was used in determining density estimates to eliminate artefactual tissue shrinkage during staining; with the microtome accuracy to cut precise sections having been previously validated (37). CEs using the modified disector technique outlined above were  $< 0.1$  for cortical thickness and  $< 0.15$  for the density of Betz cells and total neurons.

### Statistical analyses

The normality of data was tested using the Shapiro-Wilk test. Equality of variances was tested using Brown-Forsythe test. Group differences were investigated by either Welch's analysis of variance or Kruskal-Wallis test for non-Gaussian distributions, with either Games-Howell or Dunn's test, respectively, for pairwise comparisons. Regional differences to the previously reported ITC (26) were investigated by either Welch's T test or Wilcoxon rank-sum test for non-Gaussian distributions. The Pearson correlation coefficient ( $r$ ) and coefficient of determination ( $r^2$ ), or Spearman rho ( $\rho$ ) for non-Gaussian distributions, were calculated for univariate correlations to investigate relationships between AD-type pathology, microglial morphologies, and APOE  $\epsilon 4$  status. Stepwise regression models which included age, sex, brain pH, post-mortem interval, and fixation period were performed to exclude effects of potential confounders. A p-value  $< 0.05$  was considered statistically significant. All statistical analyses were performed using JMP Pro 14 (SAS Institute Inc). Graphs were produced using Microsoft Excel.

## Results

### The Alzheimer's disease primary motor cortex exhibits mild tau and $\beta$ -amyloid deposition but no evidence of neurodegeneration

This study involved 23 autopsy cases that had previously been clinicopathologically characterised as 'probable AD' or controls based on ABC score and clinical dementia rating (Table 1) (39). AD cases (n=8) included individuals with an intermediate-high likelihood of AD dementia following routine neuropathological diagnostic testing (38) and who presented with typical AD dementia prior to death. 'High pathology controls' (HPC) (n=5) were grouped as such on the basis of no cognitive impairment but satisfied a diagnosis of intermediate AD likelihood on post-mortem examination. Controls (n=10) included individuals with a range of ABC scores (A0–3; B0–2; C0–3), though only satisfying a 'Not' or 'Low' outcome after diagnostic testing.

There was no cortical atrophy (Fig. 1a) or neuronal loss (Fig. 1b), including the prominent layer Vb Betz cells (Fig. 1c), in the PMC of AD cases or HPCs compared with controls. Following a positive pixel analysis, grey matter A $\beta$  areal fraction (% A $\beta$ ) was higher in the PMC of AD cases compared to controls ( $p = 0.0005$ ), but not HPCs ( $p = 0.07$ ). The density of total A $\beta$  plaques, fibrillar, and dense-cored plaques was also significantly higher in AD cases compared to controls (Total  $p = 0.003$ ; Fibrillar  $p = 0.002$ ; Dense-cored  $p = 0.004$ ) but not HPCs (Total  $p = 0.1$ ; Fibrillar  $p = 0.06$ ; Dense-cored  $p = 0.2$ ). Total tau areal frac-

tion (% TTau) and the density of NFTs was higher in the PMC of AD cases compared to controls ( $^{TTau}p = 0.001$ ;  $^{NFT}p = 0.001$ ) and HPCs ( $^{TTau}p = 0.007$ ;  $^{NFT}p = 0.01$ ) (Table 2).

Amongst the AD cases, the PMC had significantly reduced % A $\beta$  ( $p = 0.006$ ), total A $\beta$  plaques (0.001), and fibrillar plaques ( $p = 0.0002$ ), but not dense-cored plaques ( $p = 0.2$ ) compared to the ITC. The % TTau ( $p = 0.02$ ) and the density of NFTs ( $p = 0.02$ ) were also significantly reduced in the PMC compared to the ITC of AD cases. Amongst controls the % TTau was significantly reduced in the PMC compared to the ITC ( $p = 0.04$ ). There were no other regional differences in terms of pathological load in controls, including amongst HPCs (Table 3).

In the ITC, all of the control, HPC, and AD cases had neuritic tau pathology at varied levels. A $\beta$  pathology in the ITC occurred in 4/10 controls, and all HPCs and AD cases. The clustering of activated microglia in the ITC was apparent in 6/10 controls (including three with only tau pathology), and all of the HPCs and AD cases except one (M12) (ITC case data is shown in Fig. 1d). In the PMC, neuritic tau pathology was present in 7/10 controls, 4/5 HPCs, and all AD cases, while A $\beta$  deposition in the PMC occurred in 6/10 controls, 4/5 HPCs, and all AD cases. Microglial clustering in the PMC was observed in 5/10 controls, and all of the HPCs and AD cases, with the exception of one case (M12) (PMC case data is shown in Fig. 1e). In controls, the % TTau correlated with age in the PMC ( $r^2 = 0.44$ ,  $p = 0.04$ ) but not in the ITC, which was near significant ( $r^2 = 0.39$ ,  $p = 0.05$ ).

**Table 2. Summary of neuronal and neuropathological data of the primary motor cortex<sup>a</sup>**

	Control	HPC	AD	P-value <sup>b</sup>
Cortical thickness (mm)	2.7 ± 0.4	3 ± 0.5	3 ± 0.4	0.3
Total neurons ('000/mm <sup>3</sup> ) <sup>c</sup>	24.8 ± 5.9	35.6 ± 12.1	33.1 ± 8	0.05
Betz cells (/mm <sup>3</sup> ) <sup>d</sup>	726.8 ± 372.5	943.7 ± 148.8	636.8 ± 265.7	0.2
% A $\beta$	0.1 ± 0.1	0.3 ± 0.3	0.7 ± 0.2	0.0009
Total A $\beta$ plaques (/mm <sup>3</sup> )	3.1 ± 4.8	4.6 ± 3.6	13.7 ± 4.7	0.003
Fibrillar (/mm <sup>3</sup> )	1.6 ± 2.2	2.2 ± 2.4	7.7 ± 4.3	0.001
Dense-cored (/mm <sup>3</sup> )	1.5 ± 3.2	2.2 ± 2.2	6 ± 2.8	0.006
% TTau	0.003 ± 0.003	0.002 ± 0.003	0.9 ± 0.6	0.004
NFTs (mm <sup>3</sup> )	0 ± 0	0 ± 0	11.8 ± 10.2	0.0004

<sup>a</sup>Mean ± standard deviation.

<sup>b</sup>ANOVA results; see text for p-values of pairwise comparisons.

<sup>c</sup>Inclusive of Betz cells.

<sup>d</sup>Density of Betz cells in layer V.

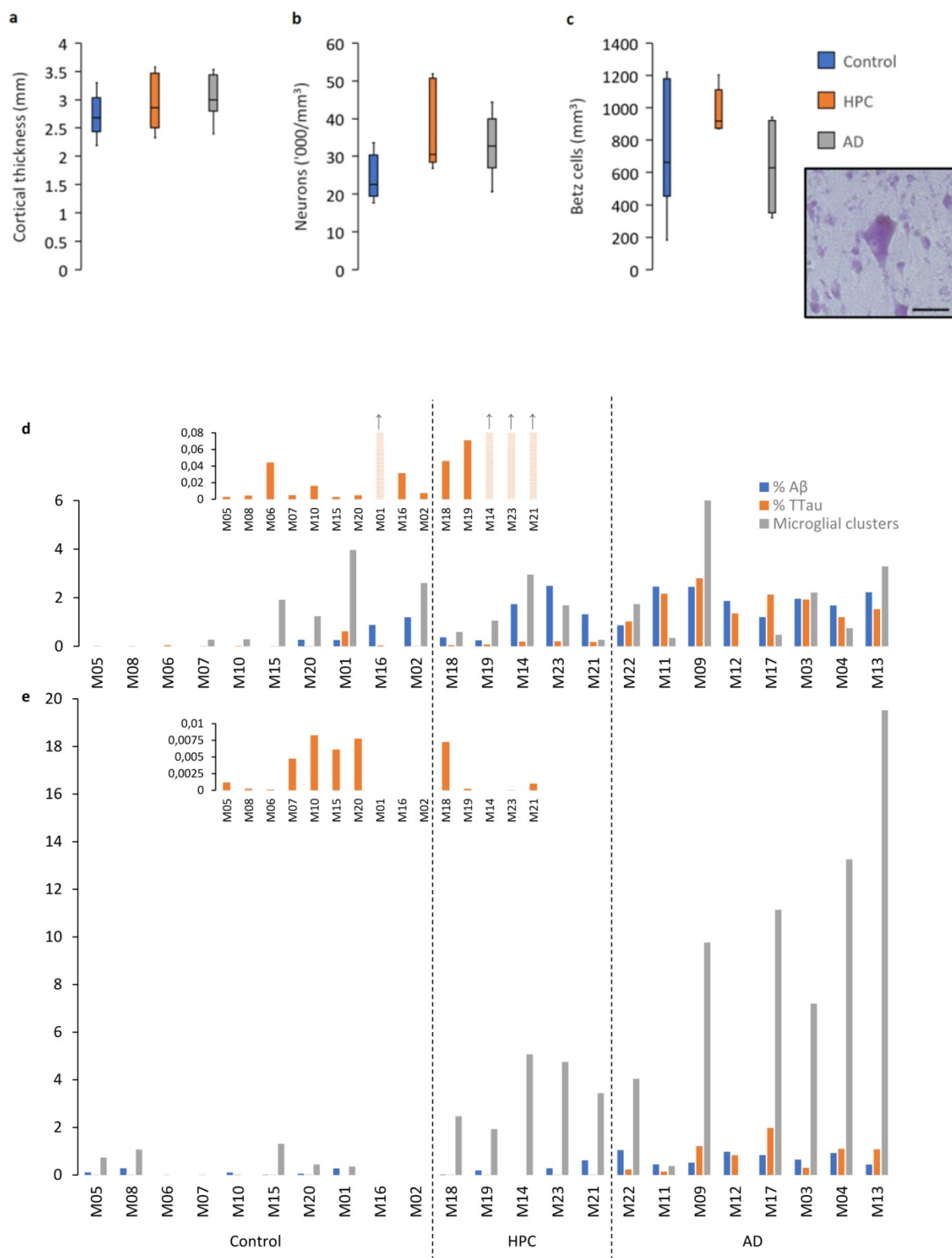


**Figure 1** Characteristics of the PMC and regional neuropathological comparisons. **a–c** The PMC is spared of AD-related neurodegenerative changes as measured by cortical thickness (**a**), total neuronal density (**b**), and the density of layer Vb Betz cells (inset demonstrates a pyramidal Betz cell with multiple asymmetrically distributed perisomatic neurites, a prominent nucleolus, and a dark dense deposit of cytoplasmic lipofuscin) (**c**). **d–e** A cohort wide comparison of the percentage of Aβ and Ttau immunolabelling and microglial clustering in the ITC (**d**) and PMC (**e**) demonstrates age-related tau build-up in a majority of control brains in both regions and an early build-up of Aβ in HPCs (that were scored as A2-3, B2, C0-3 on diagnostic slides) with a concomitant microglial clustering response that is more prevalent in the PMC compared to the ITC and which appears to dissipate with severe AD pathology in the ITC. Scale bar = 50 μm (**c**)

**Table 3. Regional neuropathological comparisons<sup>a</sup>.**

Tau		Control		
		PMC	ITC	P-value
	% TTau	0.003 ± 0.003	0.1 ± 0.2	0.04
	Tangles (/mm <sup>2</sup> )	0 ± 0	0.9 ± 2.2	0.5
		HPC		
	% TTau	0.002 ± 0.003	0.1 ± 0.1	0.06
	Tangles (/mm <sup>2</sup> )	0 ± 0	0.4 ± 0.5	0.5
		AD		
	% TTau	0.9 ± 0.6	1.8 ± 0.6	0.02
	Tangles (/mm <sup>2</sup> )	11.8 ± 10.2	21.9 ± 19.1	0.02
Aβ		Control		
	% Aβ	0.1 ± 0.1	0.3 ± 0.4	0.8
	Total Aβ plaques (/mm <sup>2</sup> )	3.1 ± 4.8	7.2 ± 13.4	0.9
	Fibrillar	1.6 ± 2.2	5.7 ± 11.3	0.9
	Dense-cored	1.5 ± 3.2	1.5 ± 2.4	>0.9
		HPC		
	% Aβ	0.3 ± 0.3	1.2 ± 0.8	0.2
	Total Aβ plaques (/mm <sup>2</sup> )	4.6 ± 3.6	29 ± 23.3	0.08
	Fibrillar	2.2 ± 2.4	22.5 ± 21.9	0.1
	Dense-cored	2.2 ± 2.2	6.5 ± 4.9	0.2
		AD		
	% Aβ	0.7 ± 0.2	1.8 ± 0.5	0.006
	Total Aβ plaques (/mm <sup>2</sup> )	13.7 ± 4.7	40.6 ± 17.7	0.001
	Fibrillar	7.7 ± 4.3	35.5 ± 17.8	0.0002
	Dense-cored	6 ± 2.8	5.1 ± 3.2	0.2

<sup>a</sup>Mean ± standard deviation.

### Clusters of activated microglia are more commonly found in the PMC than the ITC of HPCs and AD cases

The density of individual activated (Fig. 2a–e), ramified (Fig. 2f), dystrophic (Fig. 2g–h), or total microglia did not differ between any of the three groups in the PMC (Table 4). Microglial clusters (Fig. 2i–j), although a small proportion of total microglia, were significantly more common in HPCs (Fig. 2k) and AD (Fig. 2l) cases compared to controls in the PMC (<sup>HPC</sup>p = 0.01; <sup>AD</sup>p = 0.04).

Clusters in the PMC were also higher than in the ITC of HPCs (p = 0.02) and AD cases (p = 0.03) (Fig. 3a), whilst the density of total (p = 0.04) and

ramified microglia (p = 0.002) were reduced in the ITC compared to the PMC of AD cases. Immunofluorescent double-labelling for Aβ and IBA1 in the PMC showed that the clusters of activated microglia, occurred preferentially within the boundaries of fibrillar Aβ plaques, with a significant correlation in a combined analysis of control and AD brains (Spearman ρ = 0.54, p = 0.006; Fig. 3a). The percentage of Aβ plaques associated with a cluster of activated microglia in the PMC ranged from a mean of 41% in controls and 43% in AD cases to 60% in HPCs, with one control (M15), two HPCs (M14 and M18), and one AD case (M13) having a higher density of microglial clusters than Aβ plaques.

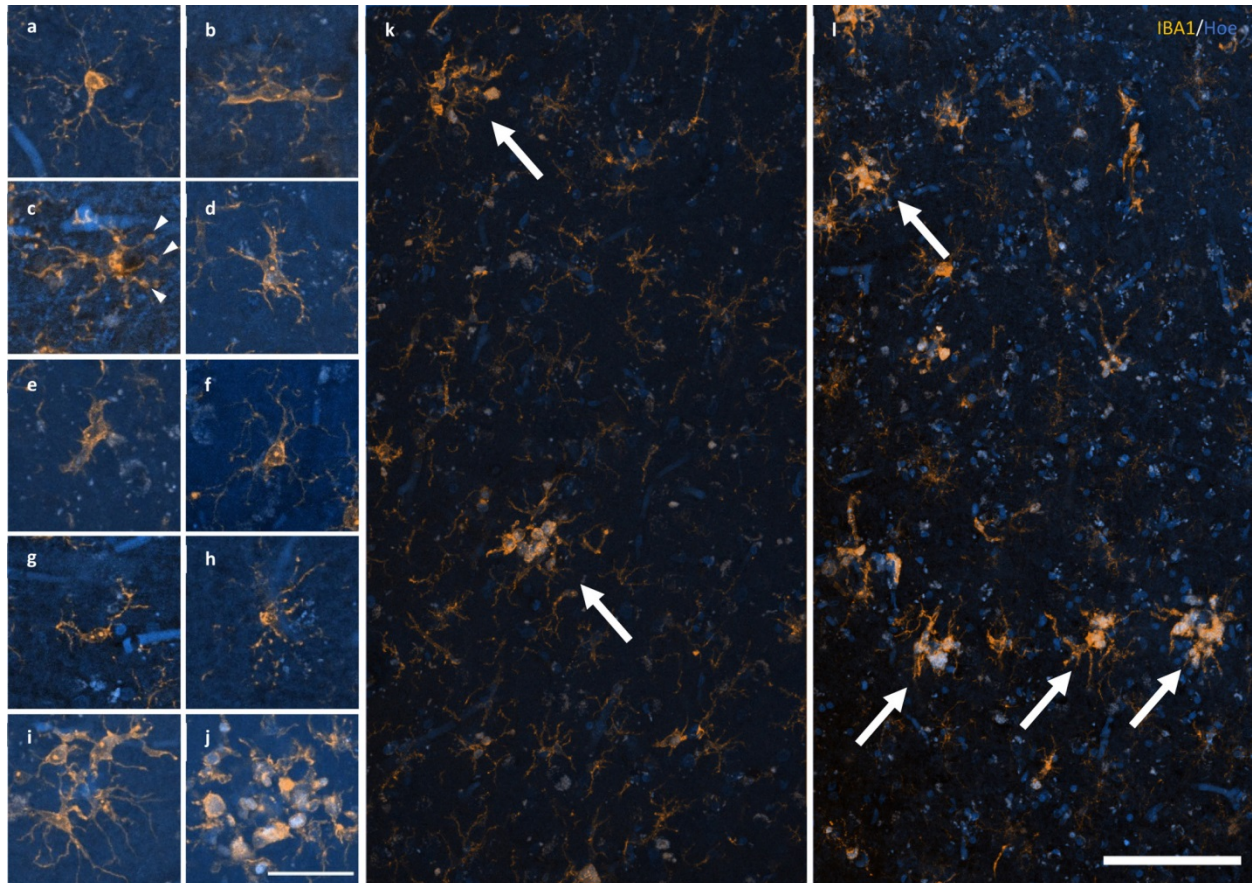


**Figure 2** Response of microglia to AD pathology. **a–e** A spectrum of microglial activation can be identified by a series of morphological changes including an enrichment of IBA1 labelling of the soma and primary processes (**a**), hypertrophy of the primary processes (**b**), retraction of tertiary processes ± the formation of morphological features consistent with phagosomes (arrow heads) (**c**), further retraction of secondary processes (**d**), until amoeboid in shape (**e**). **f–h** Healthy ramified microglia have a small, spherical soma and thin, evenly distributed processes (**f**), contrasting with dystrophic microglia that have either deramified and tortuous processes (**g**) or pseudo-fragmentation of processes when marked with IBA1 (**h**). **i–j** Microglia that form a cluster within the boundary of an Aβ plaque may be either dystrophic or have reached a phase of early (**i**) or late/amoeboid (**j**) activation. **k–l** Mosaics of IBA1 staining demonstrating the size and distribution of microglial clusters (arrows), defined as three or more somata occurring within, or touch the boundaries of, a 20 μm<sup>2</sup> virtual graticule subregion, in the PMC of an HPC (**k**; M23) and AD case (**l**; M13). Scale bar in **j** = 40 μm (**a–j**); in **l** = 100 μm (**k–l**)

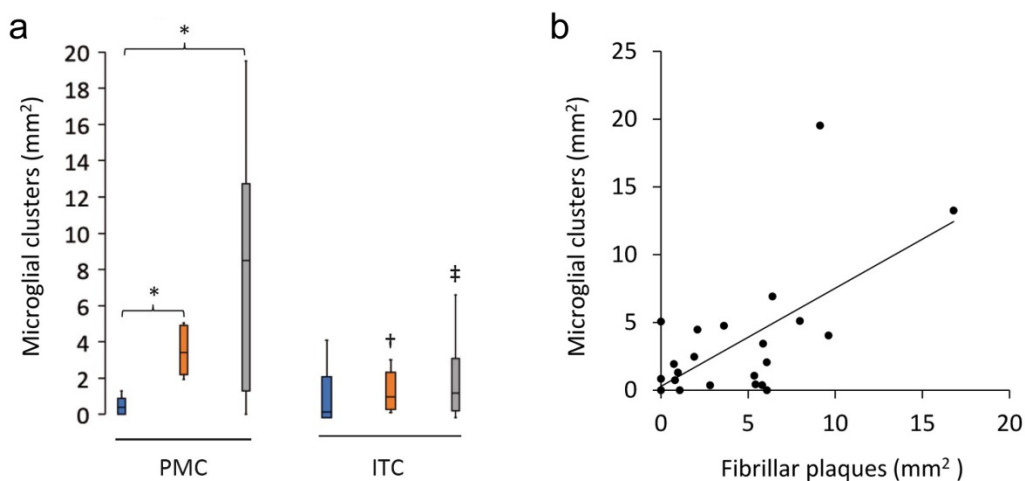


**Figure 3** Characteristics of microglial clustering in the PMC. **a** The density of microglial clusters was significantly greater in the PMC of HPCs and AD cases compared to controls. **b** Microglial clusters were more frequently associated with fibrillar neuritic plaques in a combined group analysis; Spearman  $\rho = 0.54$ ,  $p = 0.006$ . †Significantly reduced compared to PMC of HPCs; ‡Significantly reduced compared to PMC of AD cases. \*\*\* $p < 0.05$ .

**Table 4. Quantification of the morphological subtypes of microglia in the primary motor cortex<sup>a</sup>**

	Control	HPC	AD	P-value <sup>b</sup>
Total microglia	177.4 ± 44.9	224.8 ± 67.1	195.1 ± 60.1	0.3
Ramified microglia	77.4 ± 47.3	78.3 ± 43.2	59.1 ± 27.8	0.6
Activated microglia	57 ± 31.5	96.4 ± 35.9	76.9 ± 40.9	0.1
Dystrophic microglia	43 ± 27.1	50.1 ± 26.9	59.2 ± 14.9	0.2
Microglial clusters	0.5 ± 0.5	3.5 ± 1.4	8.2 ± 6.7	0.01

<sup>a</sup>Cells/mm<sup>2</sup>; mean ± standard deviation.

<sup>b</sup>ANOVA results; see text for p-values of pairwise comparisons of microglial clusters.

### A graded extent of neuritic tau pathology and clustering of microglia occurs within nascent A $\beta$ plaques, with the persistence of dystrophic neurites and the loss of IBA1-immunoreactivity and A $\beta$ -immunoreactivity occurring in established neuritic plaques

All of the A $\beta$  plaques examined in the ITC, and a majority in the PMC, contained DNs. However, the extent of the accumulated neuritic tau pathology within each plaque was lower in the PMC (Fig. 4a) than the ITC of the same case (Fig. 4b). Both A $\beta$  deposits and globular DNs were seen perivascularly (Fig. 4c), consistent with previous observations (39). The density of DNs was greatest in the ITC of AD cases (Fig. 4c), which also had the highest density of remnant plaques characterised by accumulations of DNs associated with weak or absent A $\beta$ -immunoreactivity (Fig. 4d). In the ITC a diffuse lattice of elongated NTs occurred throughout the neuropil and independently of A $\beta$  plaques (Fig. 4e). DNs appeared radially projecting from A $\beta$  plaques (Fig. 4e) and showed either elongated or globular morphology (Fig. 5a). Hoechst dye marked cell nuclei around the periphery of A $\beta$  plaques and also partly stained the fibrillar deposits of A $\beta$  (Fig. 5a). Hoechst has previously been reported to stain A $\beta$  plaques in transgenic mice (40). Immunofluorescent double-labelling showed no colocalisation of A $\beta$  and T $\tau$  (Fig. 5b).

### Microglia cell processes exhibiting evidence of phagocytic activity are interspersed around the periphery and core of A $\beta$ plaques

Microglia that occurred in proximity to diffuse, fibrillar, and cored plaques commonly displayed structures morphologically consistent with phagosomes on distal processes with enriched IBA1 im-

munolabelling that closely associated with the A $\beta$  element in the periphery and core of plaques (Fig. 6a; Fig. 7a). As previously reported for the ITC, superior frontal gyrus, and primary visual cortex, the overall density of dystrophic microglia was inversely correlated with brain pH in the PMC ( $r^2 = 0.3$ ,  $p = 0.01$ ) (26). However, it was also noted that individual plaques with dense DNs, that were associated with weak or absent A $\beta$  staining which were more abundant in the ITC, were associated with dystrophic microglia (Fig. 6b) rather than a cluster of activated microglia which more commonly occurred where the extent of DNs was not yet fully developed (Fig. 6c–d). Confocal views showed colocalisation of microglial cell processes with A $\beta$  in AD (Fig. 7a–b), but no colocalisation with tau pathology (Fig. 7c–d).

## Discussion

AD is a uniquely human disease with a long prodrome and has proved difficult to model. The combination of using different regions of post-mortem brain tissue from individuals with or without dementia and with variable amounts of AD-type pathology may allow the pathological sequence of events to be elucidated. For example, the level of disease severity could be ordered from lowest to highest as follows: PMC-controls < ITC-controls < PMC-HPC < ITC-HPC < PMC-AD < ITC-AD. In particular, regions such as the ITC in HPCs and the PMC in AD cases could harbour the pre-symptomatic targets required to therapeutically delay or prevent AD. Prior to using this model to understand the role of microglia in AD, a quantitative neuropathological analysis of the PMC was carried out to ensure that it met expectations for being a relatively unaffected region of the AD brain.

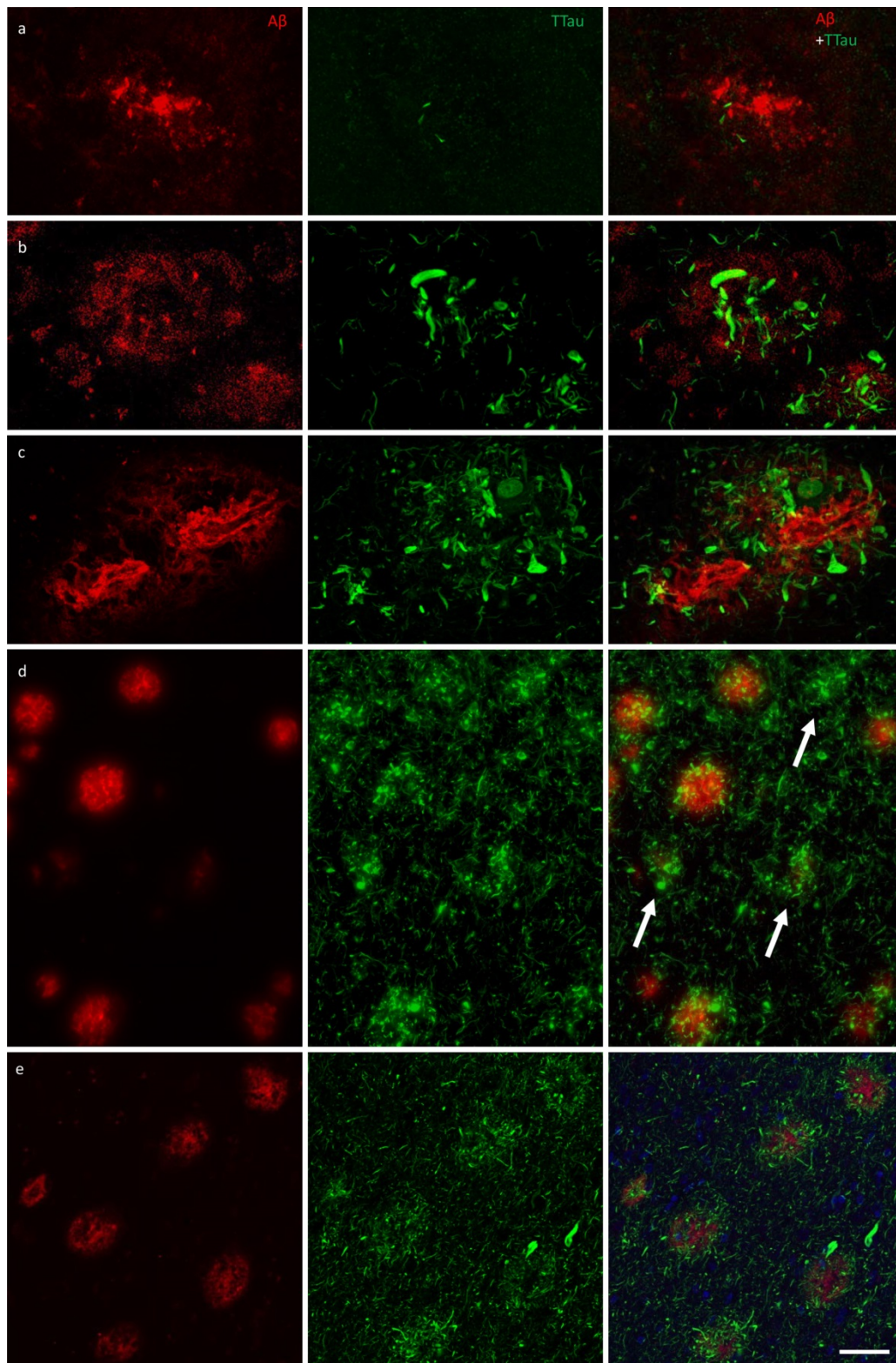


**Figure 4** Immunofluorescent double-labelling for A $\beta$  and Ttau. **a–c** The majority of A $\beta$  plaques examined here were associated tau-positive dystrophic neurites, with a clear gradation visible between the PMc (**a**) and ITC (**b**) in controls (M01 pictured in **a** and **b**) and AD cases (ITC of M09 pictured in **c**). AD cases had the most extensive build-up of DNs in fibrillar and dense-cored plaques, as well as perivascular (capillary) A $\beta$  deposits (**c**). **d** Remnant plaques (arrows) are characterised by absent or weak A $\beta$  staining and dense accumulations of tau pathology and were much more common in the ITC than the PMc (also seen in **b**). **e** Severely affected regions of the AD brain, such as the ITC, showed a diffuse network of elongated NTs throughout the parenchyma as well radially projecting DNs. Scale bar = 20  $\mu$ m (**a–c**), 60  $\mu$ m (**d**), 40  $\mu$ m (**e**)

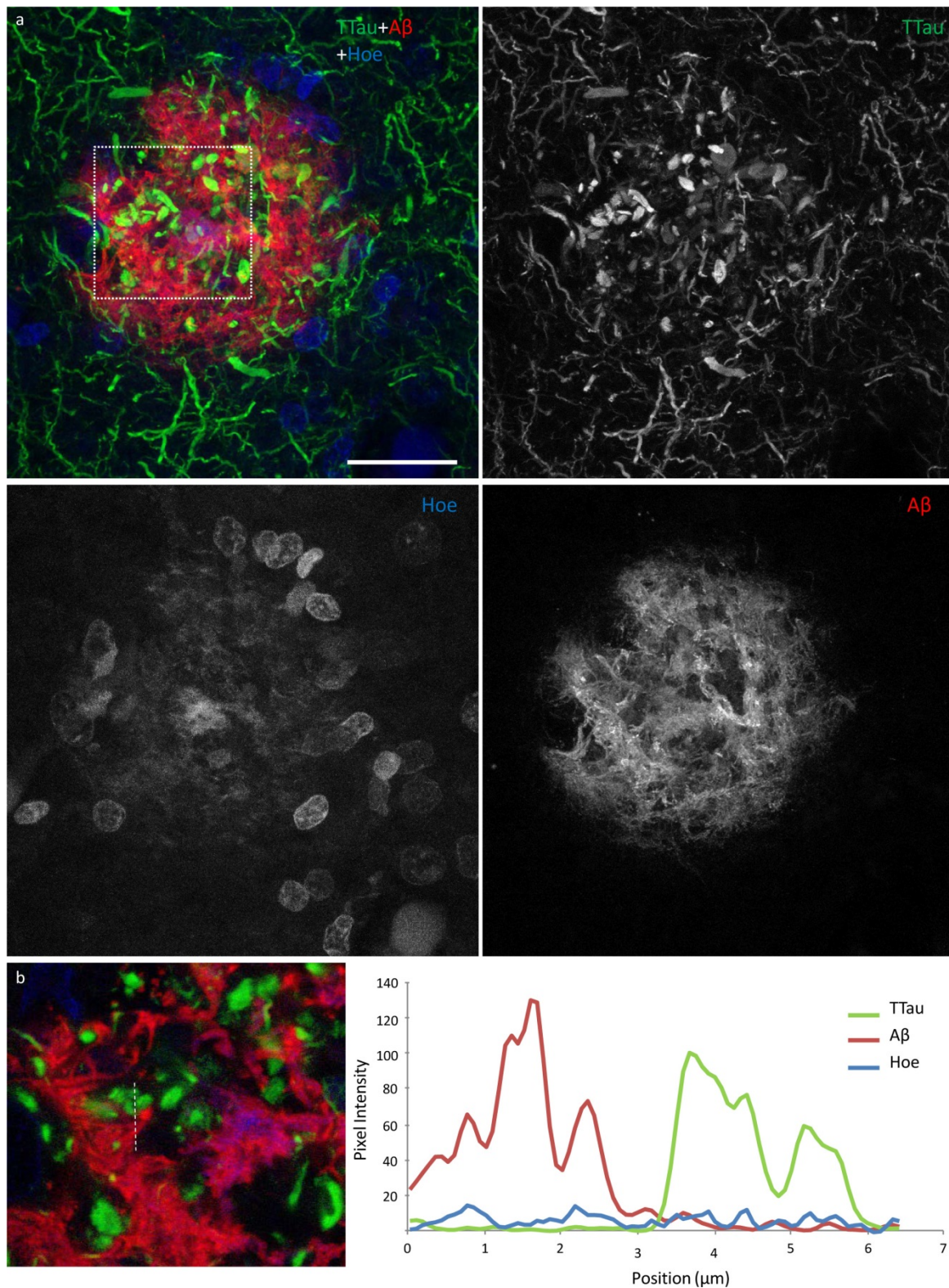


**Figure 5** High power image of an A $\beta$  plaque in AD. **a** Image panel showing a fibrillar neuritic plaque in an AD case (M03) with globular and threadlike DNs distributed throughout the plaque, which is also surrounded by a network of NTs (dotted box in merged image demonstrates ROI shown in **b**). Hoechst staining labelled cell nuclei around the periphery of the plaque as well as the fibrillar A $\beta$  component inside the plaque. **b** Colocalisation study showed no coincidence A $\beta$  and TTau staining in any of the sections examined here (dotted line represents a 6.5  $\mu$ m length along which pixel intensities have been compared in this exemplar ROI). Scale bar = 20  $\mu$ m (**a**)

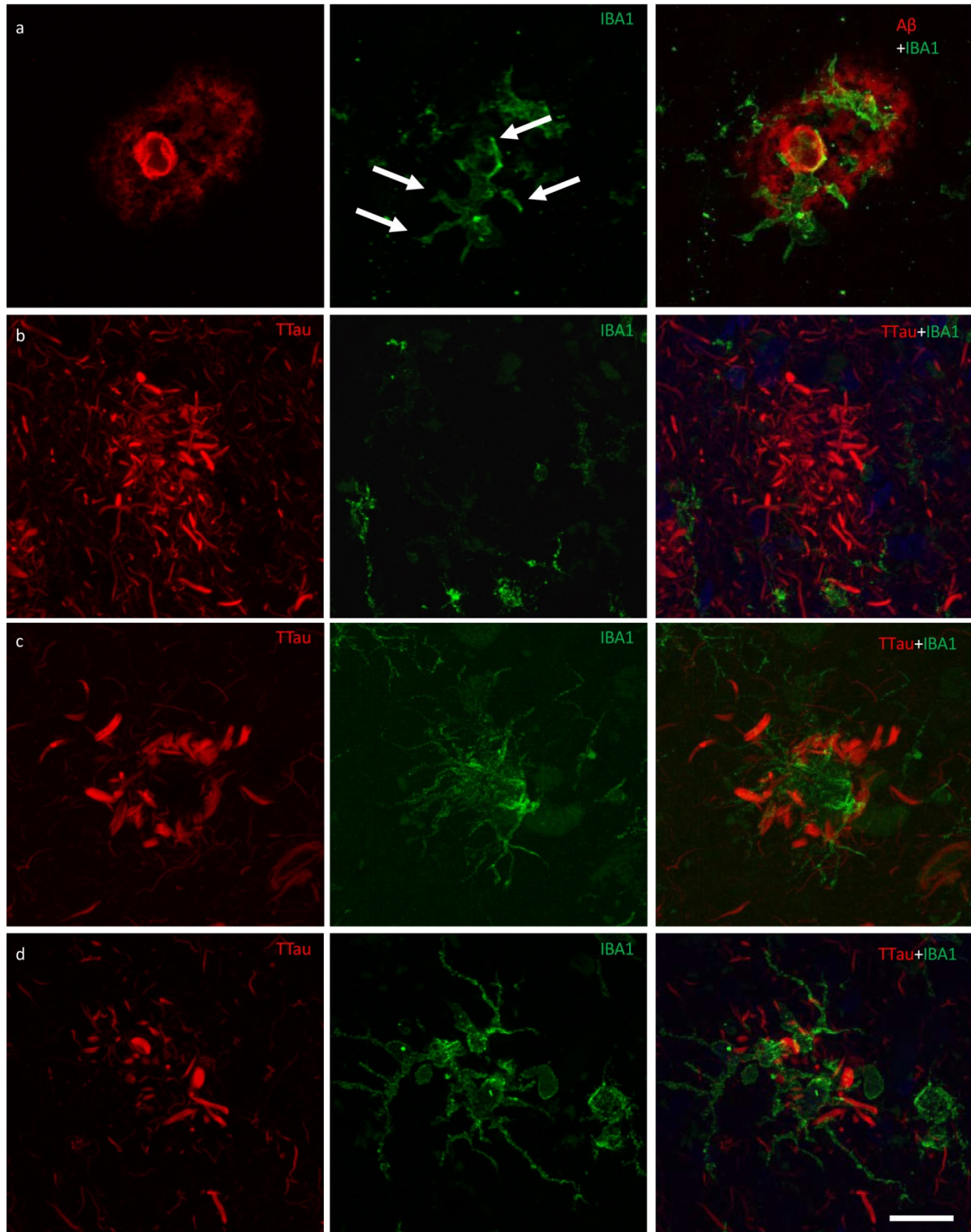


**Figure 6** Responses of microglia to AD neuropathology. **a** The ITC of a control case (M01) demonstrating activated microglia with morphological features consistent with the formation of phagosomes (arrows) responding to peripheral and core elements of an A $\beta$  plaque. **b** In the ITC of AD cases (M17 pictured), dystrophic microglia were more commonly associated with plaques that contained dense accumulations of dystrophic neurites, however the overall density of dystrophic microglia was inversely correlated with brain pH and not with AD. **c–d** Conversely, plaques with a lower density of dystrophic neurites were more commonly associated with a cluster of activated microglia (M01 pictured) in both the PMC (**c**) and ITC (**d**). Scale bar = 20  $\mu$ m (**a–d**)

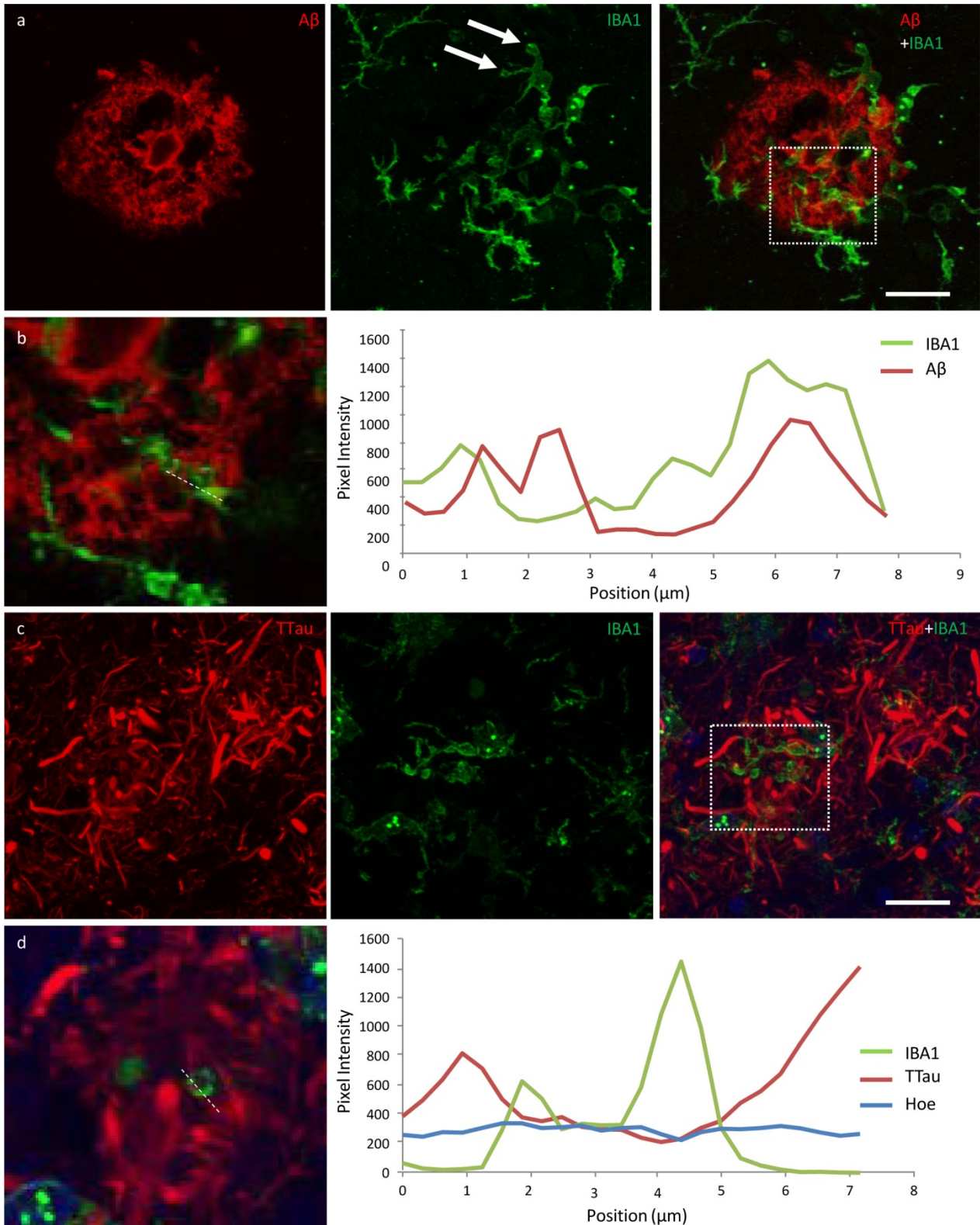


**Figure 7** Exemplars from an investigation into the potential internalisation of A $\beta$  and tau pathology by microglia. **a** Activated microglia in an A $\beta$  plaque in the ITC of a control case with morphological features consistent with the formation of phagosomes (arrows) (M01; dotted box represents region of interest in **b**). **b** Coincidence of A $\beta$  and IBA1 pixel intensities along a 7.8  $\mu\text{m}$  length (dotted line) suggests potential internalisation of A $\beta$  by microglia. **c** Activated microglia in close proximity to tau-positive DNs in the ITC of an AD case (M17; dotted box represents region of interest in **d**). **d** There was no evidence of the internalisation of tau pathology by microglia in any of the sections investigated here; exemplar shows A $\beta$  and TTau staining intensities over a 7.2  $\mu\text{m}$  length (dotted line). Scale bar 20  $\mu\text{m}$  (**a**, **c**)

As expected, the PMC of AD cases had a significantly higher % A $\beta$ , A $\beta$  plaque count, % T $\tau$ , and NFT density compared controls. There were no NFTs observed in the PMC of controls and HPCs, which also had very similar levels of % T $\tau$  (which correlated with increasing age), but differed in their level of % A $\beta$ . HPCs were defined according to standard neuropathological diagnostic criteria – having an intermediate ABC score (38). Incidentally, HPCs and AD cases (intermediate–high ABC scores) were similar in their A $\beta$  load but differed in their tau levels in both regions. In contrast to the primary visual cortex previously investigated (26), the PMC in AD did have significantly reduced levels of A $\beta$  and overall tau pathology, including NFTs as well evidenced elsewhere (41-46), compared to the ITC of the same cases. Overall there was no evidence of neurodegeneration in the PMC of AD cases, unlike the ITC, with cortical thickness, number of total neurons, and giant layer Vb pyramidal Betz cells remaining unchanged as expected (47, 48).

Examination of the microglial morphologies in the PMC using the previously validated modified disector sampling approach across all cortical laminae yielded no significant differences between controls, HPCs, and AD cases. However, group differences could be seen locally around AD-type pathology within the cortex with an increase in clustering of activated microglia in the PMC of HPCs compared to controls, and in the PMC compared to the ITC of AD cases. Moreover, a higher percentage of plaques contained clusters of microglia in HPCs than in AD cases and also a portion of microglia clusters that were not spatially associated with A $\beta$ . The presence of a strong microglial clustering response in the PMC of AD cases and in the HPCs aligns with PET imaging studies demonstrating early activation of microglia in preclinical AD cases (49). Although the presence of clusters unrelated to A $\beta$  pathology may be a non-specific observation, it is interesting to note that a previous animal study using a 5 $\times$ FAD model also reported the presence of microgliosis prior to the formation of insoluble A $\beta$  plaques (50), with another mouse model also indicating microglial activation in relation to synaptic dysfunction prior to A $\beta$  deposition (51).

Here it is suggested that clusters of activated microglia in the PMC represent a neuroprotective

response correlating with the deposition of A $\beta$ . We have demonstrated clusters of activated microglia that display phagocytic capabilities in the mildly affected PMC before the development of extensive tau pathology. It is conceivable that once the phagocytic potential of microglia is overwhelmed, a transition to a more neurotoxic proinflammatory phenotype occurs and that this represents a pivotal moment preceding tau-related neurofibrillary degeneration. Studies in mouse models of A $\beta$  overexpression suggest proinflammatory microglia, which may be induced by the binding of oligomeric and fibrillar A $\beta$  species to NLR Family Pyrin Domain Containing 3, Receptor for Advanced Glycation Endproducts, Scavenger receptors, and Toll-like receptors, among others (52-58), are associated with poorer cognitive and survival outcomes, have impaired phagocytic capabilities (59), and are capable of secreting an expansive complement of neurotoxic compounds including reactive oxygen species, nitric oxide, peroxynitrite, tumour necrosis factor  $\alpha$ , interleukin 1  $\beta$ , and prostaglandin-E2 (60). However A $\beta$ -independent mechanisms of microglia activation or exhaustion in human AD cannot be excluded and require further research considering the so far limited efficacy of the pharmacological clearance of A $\beta$  in clinical trials (61, 62).

Activated microglia tended to be associated with fibrillar NPs, and higher resolution confocal photomicrographs showed evidence of A $\beta$  internalisation by microglia in both regions. The latter may explain the remnant plaques observed here (that contain weak or absent A $\beta$ -immunolabelling; in which higher levels of A $\beta$  were associated with activated microglia, but dystrophic microglia where A $\beta$ -immunoreactivity was very minimal or absent, particularly where dystrophic neurites were extensive) and described elsewhere (14) and is potentially relevant to the proposed dynamic equilibrium between soluble A $\beta$  oligomers and insoluble fibrils (63). However, it will be important to confirm the internalisation of A $\beta$  by microglia with super resolution techniques such as direct stochastic optical reconstruction microscopy (dSTORM). In contrast, microglia did not specifically cluster around any of the three forms of tau pathology, NFTs, NTs and DNs, nor did they appear to internalise tau in colocalisation studies, although processes of microglia were coincidentally found adjacent to DNs. The

microglial clustering response dissipated over the modelled disease course with advanced stages, represented by the ITC of AD cases, being characterised by reduced IBA1 immunoreactivity, as reported elsewhere (31, 64). This suggests a process of microglial incapacitation in the context of increased tau load, a concept which is supported by a growing body of literature (65, 66). From these results it is hypothesised that the activation of microglia coincides with cortical A $\beta$  deposition. Neuritic inclusions of tau in the cortex are evident early in the disease process, represented here by the PMC of AD cases, but mainly develop after the deposition A $\beta$  and the activation of microglia.

This sequence of pathological changes is ostensibly consistent with the amyloid cascade hypothesis for AD pathogenesis (19) given the presence of elevated A $\beta$  in the PMC of HPCs, however it should be stressed that the levels of A $\beta$  and tau pathology were present at similar levels in the PMC of confirmed AD cases. Therefore it could be argued that insoluble A $\beta$  and tau deposits begin forming concurrently in the cerebral cortex of AD brains. This would be consistent with those arguing in favour of the pathogenetic importance of tau deposition (22, 23, 67, 68) and the possibility that it in fact acts as a causative factor behind AD-related microglial activation (69). Certainly, animal models suggest that microglial activation augments tau pathology and specifically tau phosphorylation (70). This scenario would then be consistent with our observation that microglial activation wanes with increased tau deposition and with the idea that ageing impairs the housekeeping functions of microglia (71). Finally, even in the presence of extensive tau pathology, the increased presence of remnant plaques in the ITC suggests that microglia retain the ability to clear A $\beta$  peptides.

Understanding the functional significance of these dynamic spatiotemporal changes in microglial activity along the time course of AD pathophysiology will be critical before new treatments targeting these cells can be imagined. Given that microglia of different brain regions display different activation states simultaneously depending on the graded extent of AD-type pathology present, the implementation of either anti- or pro-inflammatory microglia-based therapies would presumably be

beneficial in one brain region but detrimental in another. In future work the genetic characterisation of subjects investigated here may also provide further insight into how genotype affects individual susceptibility to differential microglial function, represented by the highly variable clustering response of microglia in HPCs and AD cases in particular. Overall, findings from the post-mortem model used here suggest that the clustering of activated microglia occurs concomitantly with the formation of A $\beta$  plaques, and that tau-related neuritic degeneration follows these changes along with a loss of clustering.

## Acknowledgements

The authors would like to thank the donors and their families for their kind gift. Brain tissue was received from the NSW Brain Tissue Resource Centre and Sydney Brain Bank. These brain banks are supported by the NHMRC of Australia, The University of New South Wales, Neuroscience Research Australia, and the National Institute of Alcohol Abuse and Alcoholism (NIH (NIAAA) R24AA012725). The authors also acknowledge the facilities used at The Bosch Institute and Microscopy Australia at the Australian Centre for Microscopy & Microanalysis both at The University of Sydney.

## Data availability statement

The data that support the findings of this study are available from the corresponding author upon reasonable request.

## References

1. Braak E, Braak H, Mandelkow EM. A sequence of cytoskeleton changes related to the formation of neurofibrillary tangles and neuropil threads. *Acta Neuropathol.* 1994;87(6):554-67.
2. Perry G, Kawai M, Tabaton M, Onorato M, Mulvihill P, Richey P, et al. Neuropil threads of Alzheimer's disease show a marked alteration of the normal cytoskeleton. *J Neurosci.* 1991;11(6):1748-55.
3. Barghorn S, Davies P, Mandelkow E. Tau paired helical filaments from Alzheimer's disease brain and assembled in vitro are based on beta-structure in the core domain. *Biochemistry.* 2004;43(6):1694-703.
4. Fitzpatrick AWP, Falcon B, He S, Murzin AG, Murshudov G, Garringer HJ, et al. Cryo-EM structures of tau filaments from Alzheimer's disease. *Nature.* 2017;547(7662):185-90.
5. Braak H, Braak E. Neuropathological staging of Alzheimer-related changes. *Acta Neuropathol.* 1991;82(4):239-59.
6. Franzmeier N, Neitzel J, Rubinski A, Smith R, Strandberg O, Ossenkoppele R, et al. Functional brain architecture is associated with the rate of tau accumulation in Alzheimer's disease. *Nat Commun.* 2020;11(1):347.
7. Nelson PT, Alafuzoff I, Bigio EH, Bouras C, Braak H, Cairns NJ, et al. Correlation of Alzheimer disease neuropathologic changes with cognitive status: a review of the literature. *J Neuropathol Exp Neurol.* 2012;71.
8. Arriagada PV, Growdon JH, Hedley-Whyte ET, Hyman BT. Neurofibrillary tangles but not senile plaques parallel duration and severity of Alzheimer's disease. *Neurology.* 1992;42(3 Pt 1):631-9.
9. Thal DR, Rub U, Orantes M, Braak H. Phases of A beta-deposition in the human brain and its relevance for the development of AD. *Neurology.* 2002;58(12):1791-800.
10. Serrano-Pozo A, Mielke ML, Gomez-Isla T, Betensky RA, Growdon JH, Frosch MP, et al. Reactive glia not only associates with plaques but also parallels tangles in Alzheimer's disease. *Am J Pathol.* 2011;179(3):1373-84.
11. Mirra SS, Heyman A, McKeel D, Sumi SM, Crain BJ, Brownlee LM, et al. The Consortium to Establish a Registry for Alzheimer's Disease (CERAD). Part II. Standardization of the neuropathologic assessment of Alzheimer's disease. *Neurology.* 1991;41(4):479-86.
12. Dickson TC, Vickers JC. The morphological phenotype of beta-amyloid plaques and associated neuritic changes in Alzheimer's disease. *Neuroscience.* 2001;105(1):99-107.
13. Yasuhara O, Kawamata T, Aimi Y, McGeer EG, McGeer PL. Two types of dystrophic neurites in senile plaques of Alzheimer disease and elderly non-demented cases. *Neurosci Lett.* 1994;171(1-2):73-6.
14. Oide T, Kinoshita T, Arima K. Regression stage senile plaques in the natural course of Alzheimer's disease. *Neuropathol Appl Neurobiol.* 2006;32(5):539-56.
15. Yu L, Petyuk VA, Tasaki S, Boyle PA, Gaiteri C, Schneider JA, et al. Association of Cortical beta-Amyloid Protein in the Absence of Insoluble Deposits With Alzheimer Disease. *JAMA Neurol.* 2019.
16. Lesne SE, Sherman MA, Grant M, Kuskowski M, Schneider JA, Bennett DA, et al. Brain amyloid-beta oligomers in ageing and Alzheimer's disease. *Brain.* 2013;136(Pt 5):1383-98.
17. Lue LF, Kuo YM, Roher AE, Brachova L, Shen Y, Sue L, et al. Soluble amyloid beta peptide concentration as a predictor of synaptic change in Alzheimer's disease. *Am J Pathol.* 1999;155(3):853-62.
18. McLean CA, Cherny RA, Fraser FW, Fuller SJ, Smith MJ, Beyreuther K, et al. Soluble pool of Abeta amyloid as a determinant of severity of neurodegeneration in Alzheimer's disease. *Ann Neurol.* 1999;46(6):860-6.
19. Selkoe DJ, Hardy J. The amyloid hypothesis of Alzheimer's disease at 25 years. *EMBO Mol Med.* 2016;8(6):595-608.
20. Hardy J, Selkoe DJ. The amyloid hypothesis of Alzheimer's disease: progress and problems on the road to therapeutics. *Science.* 2002;297(5580):353-6.
21. Braak H, Del Tredici K. The pathological process underlying Alzheimer's disease in individuals under thirty. *Acta Neuropathol.* 2011;121(2):171-81.
22. Braak H, Thal DR, Ghebremedhin E, Del Tredici K. Stages of the pathologic process in Alzheimer disease: age categories from 1 to 100 years. *J Neuropathol Exp Neurol.* 2011;70(11):960-9.
23. Streit WJ, Braak H, Del Tredici K, Leyh J, Lier J, Khoshbouei H, et al. Microglial activation occurs late during preclinical Alzheimer's disease. *Glia.* 2018;66(12):2550-62.
24. Crary JF, Trojanowski JQ, Schneider JA, Abisambra JF, Abner EL, Alafuzoff I, et al. Primary age-related tauopathy (PART): a common pathology associated with human aging. *Acta Neuropathol.* 2014;128(6):755-66.
25. Kettenmann H, Hanisch UK, Noda M, Verkhratsky A. Physiology of microglia. *Physiol Rev.* 2011;91.
26. Paasila PJ, Davies DS, Kril JJ, Goldsbury C, Sutherland GT. The relationship between the morphological subtypes of microglia and Alzheimer's disease neuropathology. *Brain Pathol.* 2019.
27. Bachstetter AD, Van Eldik LJ, Schmitt FA, Neltner JH, Ighodaro ET, Webster SJ, et al. Disease-related microglia heterogeneity in the hippocampus of Alzheimer's disease, dementia with Lewy bodies, and hippocampal sclerosis of aging. *Acta Neuropathol Commun.* 2015;3:32.
28. Streit WJ, Walter SA, Pennell NA. Reactive microgliosis. *Prog Neurobiol.* 1999;57(6):563-81.
29. Streit WJ, Sammons NW, Kuhns AJ, Sparks DL. Dystrophic microglia in the aging human brain. *Glia.* 2004;45(2):208-12.
30. Streit WJ, Braak H, Xue QS, Bechmann I. Dystrophic (senescent) rather than activated microglial cells are associated with tau pathology and likely precede neurodegeneration in Alzheimer's disease. *Acta Neuropathol.* 2009;118(4):475-85.
31. Tischer J, Krueger M, Mueller W, Staszewski O, Prinz M, Streit WJ, et al. Inhomogeneous distribution of Iba-1 characterizes microglial pathology in Alzheimer's disease. *Glia.* 2016;64(9):1562-72.
32. Sanchez-Mejias E, Navarro V, Jimenez S, Sanchez-Mico M, Sanchez-Varo R, Nunez-Diaz C, et al. Soluble phospho-tau from Alzheimer's disease hippocampus drives microglial degeneration. *Acta Neuropathol.* 2016;132(6):897-916.
33. Walker DG, Tang TM, Mendsaikhan A, Tooyama I, Serrano GE, Sue LI, et al. Patterns of Expression of Purinergic Receptor P2RY12, a Putative Marker for Non-Activated Microglia, in Aged and Alzheimer's Disease Brains. *Int J Mol Sci.* 2020;21(2).
34. Davies DS, Ma J, Jegathees T, Goldsbury C. Microglia show altered morphology and reduced arborization in human brain during aging and Alzheimer's disease. *Brain Pathol.* 2017;27(6):795-808.
35. Sutherland GT, Sheedy D, Stevens J, McCrossin T, Smith CC, van Rooijen M, et al. The NSW brain tissue resource centre: Banking for alcohol and major neuropsychiatric disorders research. *Alcohol.* 2016:33-9.

36. Rahman T, Davies DS, Tannenberg RK, Fok S, Shepherd C, Dodd PR, et al. Cofilin rods and aggregates concur with tau pathology and the development of Alzheimer's disease. *J Alzheimers Dis*. 2014;42(4):1443-60.
37. Kril JJ, Halliday GM, Svoboda MD, Cartwright H. The cerebral cortex is damaged in chronic alcoholics. *Neuroscience*. 1997;79(4):983-98.
38. Montine TJ, Phelps CH, Beach TG, Bigio EH, Cairns NJ, Dickson DW, et al. National Institute on Aging-Alzheimer's Association guidelines for the neuropathologic assessment of Alzheimer's disease: a practical approach. *Acta Neuropathol*. 2012;123(1):1-11.
39. Hansra GK, Popov G, Banaczek PO, Vogiatzis M, Jegathees T, Goldsbury CE, et al. The neuritic plaque in Alzheimer's disease: Perivascular degeneration of neuronal processes. *Neurobiology of Aging*. 2019.
40. Uchida Y, Takahashi H. Rapid detection of Abeta deposits in APP transgenic mice by Hoechst 33342. *Neurosci Lett*. 2008;448(3):279-81.
41. Murray ME, Graff-Radford NR, Ross OA, Petersen RC, Duara R, Dickson DW. Neuropathologically defined subtypes of Alzheimer's disease with distinct clinical characteristics: a retrospective study. *Lancet Neurol*. 2011;10(9):785-96.
42. Arendt T, Bruckner MK, Gertz HJ, Marcova L. Cortical distribution of neurofibrillary tangles in Alzheimer's disease matches the pattern of neurons that retain their capacity of plastic remodelling in the adult brain. *Neuroscience*. 1998;83(4):991-1002.
43. Geula C, Mesulam MM, Saroff DM, Wu CK. Relationship between plaques, tangles, and loss of cortical cholinergic fibers in Alzheimer disease. *J Neuropathol Exp Neurol*. 1998;57(1):63-75.
44. Golaz J, Bouras C, Hof PR. Motor cortex involvement in presenile dementia: report of a case. *J Geriatr Psychiatry Neurol*. 1992;5(2):85-92.
45. Petersen C, Nolan AL, de Paula Franca Resende E, Miller Z, Ehrenberg AJ, Gorno-Tempini ML, et al. Alzheimer's disease clinical variants show distinct regional patterns of neurofibrillary tangle accumulation. *Acta Neuropathol*. 2019;138(4):597-612.
46. Suva D, Favre I, Kraftsik R, Esteban M, Lobrinus A, Miklossy J. Primary motor cortex involvement in Alzheimer disease. *J Neuropathol Exp Neurol*. 1999;58(11):1125-34.
47. Arnold SE, Hyman BT, Flory J, Damasio AR, Van Hoesen GW. The topographical and neuroanatomical distribution of neurofibrillary tangles and neuritic plaques in the cerebral cortex of patients with Alzheimer's disease. *Cereb Cortex*. 1991;1(1):103-16.
48. Genç B, Jara JH, Lagrimas AKB, Pytel P, Roos RP, Mesulam MM, et al. Apical dendrite degeneration, a novel cellular pathology for Betz cells in ALS. *Scientific reports*. 2017;7:41765-.
49. Shen Z, Bao X, Wang R. Clinical PET Imaging of Microglial Activation: Implications for Microglial Therapeutics in Alzheimer's Disease. *Front Aging Neurosci*. 2018;10:314-.
50. Boza-Serrano A, Yang Y, Paulus A, Deierborg T. Innate immune alterations are elicited in microglial cells before plaque deposition in the Alzheimer's disease mouse model 5xFAD. *Scientific Reports*. 2018;8(1):1550.
51. Hong S, Beja-Glasser VF, Nfonoyim BM, Frouin A, Li S, Ramakrishnan S, et al. Complement and microglia mediate early synapse loss in Alzheimer mouse models. *Science*. 2016;352(6286):712-6.
52. Cameron B, Tse W, Lamb R, Li X, Lamb BT, Landreth GE. Loss of Interleukin Receptor-Associated Kinase 4 Signaling Suppresses Amyloid Pathology and Alters Microglial Phenotype in a Mouse Model of Alzheimer's Disease. *The Journal of Neuroscience*. 2012;32(43):15112-23.
53. Halle A, Hornung V, Petzold GC, Stewart CR, Monks BG, Reinheckel T, et al. The NALP3 inflammasome is involved in the innate immune response to amyloid-beta. *Nat Immunol*. 2008;9(8):857-65.
54. Salminen A, Ojala J, Kauppinen A, Kaarniranta K, Suuronen T. Inflammation in Alzheimer's disease: amyloid-beta oligomers trigger innate immunity defence via pattern recognition receptors. *Prog Neurobiol*. 2009;87(3):181-94.
55. Heneka MT, Kummer MP, Stutz A, Delekate A, Schwartz S, Vieira-Saecker A, et al. NLRP3 is activated in Alzheimer's disease and contributes to pathology in APP/PS1 mice. *Nature*. 2013;493(7434):674-8.
56. Heneka MT, Golenbock DT, Latz E. Innate immunity in Alzheimer's disease. *Nat Immunol*. 2015;16(3):229-36.
57. Heneka MT, Kummer MP, Latz E. Innate immune activation in neurodegenerative disease. *Nat Rev Immunol*. 2014;14(7):463-77.
58. Hanisch U-K, Kettenmann H. Microglia: active sensor and versatile effector cells in the normal and pathologic brain. *Nat Neurosci*. 2007;10(11):1387-94.
59. Koenigsnecht-Talboo J, Landreth GE. Microglial phagocytosis induced by fibrillar beta-amyloid and IgGs are differentially regulated by proinflammatory cytokines. *J Neurosci*. 2005;25(36):8240-9.
60. Block ML, Zecca L, Hong JS. Microglia-mediated neurotoxicity: uncovering the molecular mechanisms. *Nat Rev Neurosci*. 2007;8(1):57-69.
61. Howard R, Liu KY. Questions EMERGE as Biogen claims aducanumab turnaround. *Nature Reviews Neurology*. 2020;16(2):63-4.
62. Cummings J, Lee G, Ritter A, Sabbagh M, Zhong K. Alzheimer's disease drug development pipeline: 2019. *Alzheimers Dement (N Y)*. 2019;5:272-93.
63. Wang ZX, Tan L, Liu J, Yu JT. The Essential Role of Soluble A $\beta$  Oligomers in Alzheimer's Disease. *Mol Neurobiol*. 2016;53(3):1905-24.
64. Minett T, Classey J, Matthews FE, Fahrenhold M, Taga M, Brayne C, et al. Microglial immunophenotype in dementia with Alzheimer's pathology. *J Neuroinflammation*. 2016;13(1):135.
65. Streit WJ, Khoshbouei H, Bechmann I. Dystrophic microglia in late-onset Alzheimer's disease. *Glia*. 2020;68(4):845-54.
66. Navarro V, Sanchez-Mejias E, Jimenez S, Muñoz-Castro C, Sanchez-Varo R, Davila JC, et al. Microglia in Alzheimer's Disease: Activated, Dysfunctional or Degenerative. *Front Aging Neurosci*. 2018;10:140.
67. Iqbal K, Liu F, Gong CX, Alonso Adel C, Grundke-Iqbal I. Mechanisms of tau-induced neurodegeneration. *Acta Neuropathol*. 2009;118(1):53-69.
68. Grinberg LT, Rub U, Ferretti RE, Nitrini R, Farfel JM, Polichiso L, et al. The dorsal raphe nucleus shows phospho-tau neurofibrillary changes before the transentorhinal region in Alzheimer's disease. A precocious onset? *Neuropathol Appl Neurobiol*. 2009;35(4):406-16.
69. Felsky D, Roostaei T, Nho K, Risacher SL, Bradshaw EM, Petyuk V, et al. Neuropathological correlates and genetic architecture of microglial activation in elderly human brain. *Nature Communications*. 2019;10(1):409.
70. Ising C, Venegas C, Zhang S, Scheiblich H, Schmidt SV, Vieira-Saecker A, et al. NLRP3 inflammasome activation drives tau pathology. *Nature*. 2019;575(7784):669-73.
71. Vogels T, Murgoci AN, Hromadka T. Intersection of pathological tau and microglia at the synapse. *Acta neuropathologica communications*. 2019;7(1):109.